

THE PHOTODISINTEGRATION OF DEUTERIUM

Calibration of the Lund Photon Tagger

By

Vance Ryan Morrison

A thesis submitted to the

Department of Physics

Mount Allison University

in partial fulfillment of the requirements for the

Bachelor of Science degree

with Honours

May, 2006

ABSTRACT

In order to calibrate the Lund photon tagger, neutron kinetic energy was calculated from the photodisintegration of deuterium reaction. A heavy water target was used and the detectors were placed at a distance of 3.274 m and at an angle of 122.5° . The Time-Of-Flight method was used to obtain neutron energies. Due to problems in the data, proper neutron timing was not obtained and therefore the tagger was unable to be calibrated. This experiment was conducted at MAX-lab accelerator laboratory located at the University of Lund in Sweden in September 2005.

ACKNOWLEDGMENTS

I would like to thank Dr. David Hornidge for his continued assistance and guidance throughout this project. His knowledge and dedication as well as the countless hours he spent helping me were invaluable and none of this would have been possible without him.

Secondly I would like to thank Dr. Kevin Fissum of MAX-lab for everything he has done. His guidance throughout the experiment and continued assistance during the analysis was crucial. I would also like to thank the rest of the collaboration at MAX-lab for the help they've given and for making my stay in Sweden as enjoyable as it was.

Thanks to thank NSERC and Mount Allison University for their support and funding.

Finally, I would like to thank my parents for their continued support and encouragement throughout.

Contents

ABSTRACT	i
ACKNOWLEDGMENTS	ii
TABLE OF CONTENTS	iv
LIST OF FIGURES	vi
LIST OF TABLES	vii
GLOSSARY	viii
1 INTRODUCTION	1
1.1 Quantum Chromodynamics	2
1.2 Polarizabilities	3
1.3 Compton Scattering from Deuterium	5
1.4 The Photon Tagger	6
1.5 Photodisintegration of Deuterium	8
2 EXPERIMENT	11
2.1 MAX-lab Research Facility	11
2.2 The Tagging System	12
2.3 NORDBALL Array	14
2.4 Experimental Setup	16
2.5 Measurement	16
2.5.1 Neutron Time of Flight	16
2.5.2 Neutron Kinetic Energy	17
2.5.3 Pulse-Shape Discrimination	20
2.6 Electronics	22
3 ANALYSIS	27
3.1 Extraction of neutron events	27
3.2 Neutron Time Of Flight	31

4 RESULTS AND CONCLUSION	35
4.1 Conclusion	35
4.2 Future Work	36
REFERENCES	37
A Kinematics	39
B Scintillation Detectors	41
B.1 Organic Scintillation	41
B.2 Inorganic Scintillation	42
B.3 Photomultiplier Tubes	43
B.4 Pulse-Shape Discrimination	43

List of Figures

1.1	Electric and magnetic polarizabilities [Hor99].	4
1.2	Compton scattering from deuterium. $\gamma + d = \gamma + d$	7
1.3	The photodisintegration of deuterium, $\gamma + d \rightarrow p + n$	8
2.1	Bremsstrahlung energy distribution for a 135-MeV electron beam. . .	13
2.2	Schematic diagram of the Lund Tagger.	14
2.3	Schematic diagram of the NORDBALL detector arrangement.	15
2.4	Diagram of the placement of the target, veto detector and the NORDBALL detectors.	17
2.5	The γ -flash produced by relativistic events with the neutron events superimposed. Relative timing of the neutron TOF is shown [Nil06]. .	18
2.6	Scatter plot of long gate integration versus pulse shape value.	21
2.7	Circuit diagram of the data acquisition electronics.	23
3.1	Example of the software cut applied to the PS vs. PH scatterplot to eliminate gamma events. The first scatterplot shows the uncut data. The second scatterplot shows the data after the software cut has been applied.	28
3.2	Initially the bump seen here was thought to be neutron events and neutron TOF (Δt_n) was measured from the mean of the Gaussian fit shown.	29
3.3	Histogram of the scaler values from each channel of the focal plane. .	30
3.4	The D ₂ O and H ₂ O spectrum from focal plane channels 1-21. The bottom histogram is the difference between the two which were scaled were scaled by the number of photons needed to produce them. . . .	32
3.5	A histogram of the H ₂ O spectrum subtracted from the D ₂ O spectrum. A Gaussian fit was applied to channels zero to 400. The mean value and the sigma value for the fit are shown on the histogram with corresponding errors.	33

3.6 Schematic diagram showing the timing of the experiment. Δt_t is the photon time from radiator to target, Δt_n is neutron TOF, T_0 is the time at which the reaction occurs and Δt_e is electron flight from radiator to focal plane. 34

List of Tables

1.1	The four fundamental interactions of the standard model [Bei03]. . .	1
4.1	Results from the TDC spectrum analysis.	35

GLOSSARY

ADC	Analog-to-Digital Converter
CAMAC	Computer Aided Measurement And Control
CFD	Constant Fraction Discriminator
LG	Long Gate
LINAC	LINear ACcelerator
NIM	Nuclear Instrumentation Module
PH	Pulse Height
PMT	PhotoMultiplier Tube or also Phototube
PS	Pulse Shape
PSD	Pulse Shape Discrimination
QCD	Quantum ChromoDynamics
QED	Quantum ElectroDynamics
SAL	Saskatchewan Accelerator Laboratory
SG	Short Gate
TDC	Time-to-Digital Converter
TOF	Time-Of-Flight
VME	Versa Module Europe single board computer
X-arm	Non-tagger part of the experiment
X-trigger	Valid event signal provided by the experimental (X-arm) electronics. Used by the tagger electronics to produce a tagged event signal

Chapter 1

INTRODUCTION

Physics is the study of matter and energy and the interactions that occur between them. This includes the theory of the smallest sub-atomic particles to the behavior of the farthest galaxies. The forces that govern these interactions are known as the *four fundamental forces*, each of which acts on different forms of matter and at various distances. These forces include the gravitational, strong and weak nuclear, and the electromagnetic, and their relative strengths are given in Table 1.1.

Table 1.1: The four fundamental interactions of the standard model [Bei03].

Interaction	Particles Affected	Range	Relative Strength
Strong	Quarks	10^{-15} m	1
Electromagnetic	Charged particles	∞	10^{-2}
Weak	Quarks & leptons	10^{-18} m	10^{-5}
Gravitational	All	∞	10^{-39}

The electromagnetic interaction, which is mediated by photons, is the most well-understood of the four fundamental forces. The interactions of charged particles and the fields they produce have been tested experimentally to great success, and the theory has been unified with quantum theory and relativity as well as the weak force. Quantum electrodynamics (QED) is the field theory used to describe the electromagnetic interaction on the quantum level and is considered to be the best tested theory in physics [Pes95].

The other fundamental interactions have remained more difficult to understand. The gravitational interaction is well understood on the macroscopic level (describing the behavior of planets and galaxies); the current theory being Einstein's theory of

general relativity. This theory, although flawless on the macroscopic scale, has not been able to be merged with the theories describing microscopic interactions. The weak interaction acts on leptons and hadrons and is mediated by the W^+ , W^- and Z^0 bosons. These are massive particles with short lifespans that enable the weak force to be effective only over very small distances. Currently the weak interaction has been unified with the electromagnetic interaction into what is known as the *electro-weak* theory.

The strong interaction is the theory of the forces between the quarks, and describes the behavior of atomic nuclei and other subatomic particles. This interaction is the most prominent one involved in the reactions of this paper, and the current theory describing it, Quantum Chromodynamics, will be discussed in this chapter.

1.1 Quantum Chromodynamics

Quantum Chromodynamics (QCD) is the theory of the strong interaction that governs the behavior of quarks and gluons on the subatomic level [Hal84]. QCD is a quantum field theory, similar to QED. In QCD every quark is given a “colour” charge: red, green or blue, or one of the corresponding anti-colours. The colours used in QCD are, of course, completely arbitrary and have nothing to do with actual visible colours; this is just a useful analogy. According to QCD, no naturally occurring coloured particles exist—only colourless, or white, particles. These can be formed by a combination of a red, a green and a blue particle, or a colour-anticolour particle combination (e.g. blue-antiblue.)

The difficulty with applying QCD is that it is a nonlinear theory that is not analytically solvable. For other quantum field theories of weaker forces (e.g. QED), perturbation theory can be used to obtain accurate results due to the relatively weak strength of the interactions. Perturbation theory often fails, though, when applied

to QCD. At small distances, the strong interaction is quite weak, a phenomenon that has been termed asymptotic freedom, and due to the fact that the interaction increases in strength at larger distances, higher order perturbation terms can often not be ignored. Currently models of QCD exist, such as Chiral Perturbation Theory, Lattice QCD and Light Cone QCD, that can facilitate calculations.

1.2 Polarizabilities

The electric and magnetic polarizabilities of a system are a measure of the system's internal response to external electric and magnetic fields. Consider a system composed of both positively and negatively charged elements (as given in Figure 1.1). In the presence of an external electric field, \mathbf{E} , both positive and negative elements will experience the Coulomb force, but in opposite directions. This will stretch the system, inducing an electric dipole, \mathbf{p} , proportional to \mathbf{E} , with the constant of proportionality, α , being the electric polarizability. The electric polarizability is essentially a measure of the “stretchability” of the system. Now consider a system composed of randomly oriented magnetic dipoles in the presence of an external magnetic field, \mathbf{B} . This external field will cause the dipoles to align with the field as well as creating currents, inducing a net magnetic dipole, \mathbf{m} , throughout the entire system. This dipole moment is proportional to \mathbf{B} and has two components, the diamagnetic component and the paramagnetic component. The paramagnetic component, with constant of proportionality β_{para} , is caused by the dipoles in the system trying to align themselves with the external field. The diamagnetic component of the induced dipole, with constant of proportionality β_{dia} , is caused by currents created by the external field. In general, the two types of magnetic polarizability tend to cancel each other. The polarizabilities are expressed mathematically in the relationships

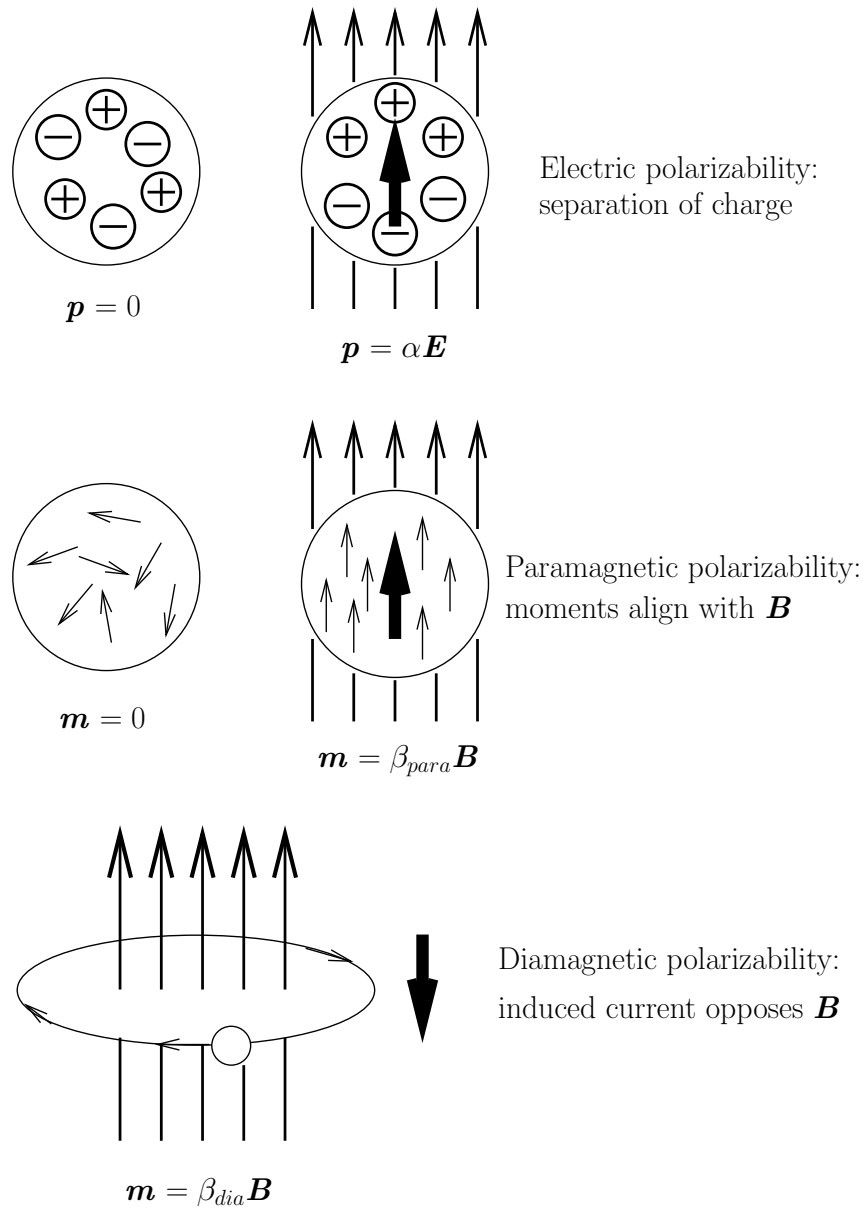


Figure 1.1: Electric and magnetic polarizabilities [Hor99].

$$\mathbf{p} = \alpha \mathbf{E} \tag{1.1}$$

$$\mathbf{m} = (\beta_{para} + \beta_{dia}) \mathbf{B}. \tag{1.2}$$

By measuring the magnitude of these polarizabilities, information about the forces binding the system together can be extracted.

1.3 Compton Scattering from Deuterium

The goal of a Compton scattering experiment on deuterium is to extract the polarizabilities of the neutron, so as to gain a better understanding of the strong force holding it together. A deuteron (which is just a deuterium nucleus) is composed solely of a proton and a neutron, so a Compton scattering reaction performed on deuterium will yield information about both the proton and the neutron. Proton polarizabilities have been studied extensively and their values are generally accepted by the scientific community. The most recent global average [Olm01] for the difference of proton polarizabilities is

$$\alpha_p - \beta_p = 10.5 \pm 0.9(\text{stat} + \text{syst}) \pm 0.7(\text{model}). \tag{1.3}$$

However, the values for the polarizabilities of the neutron are not as established as those from the protons. The most recent values available [Lun03] are

$$\alpha_n = 7.2 \pm 2.1(\text{tot}), \tag{1.4}$$

$$\beta_n = 8.1 \mp 2.1(\text{tot}). \tag{1.5}$$

Chiral Perturbation Theory provides predictions [Ber93] for neutron electric and magnetic polarizabilities with values of

$$\alpha_n = 13.0 \pm 1.5 \quad (1.6)$$

$$\beta_n = 7.8 \pm 3.6. \quad (1.7)$$

In a Compton scattering reaction, a photon is incident upon a nucleus and is reemitted with an angle, θ (see Figure 1.2). To obtain information about the polarizabilities, the differential cross-section of the Compton scattering reaction is measured. The classical differential cross-section of Compton scattering from deuterium is given by

$$\frac{d\sigma^d}{d\Omega}(\omega, \theta) = [r_0 - \omega^2(\bar{\alpha}_p + \bar{\alpha}_n)]^2 \left(\frac{1 + \cos^2\theta}{2} \right) \quad (1.8)$$

where ω is the incident photon energy, r_0 is the classical proton radius, θ is the angle of emission and $\bar{\alpha}_p$ and $\bar{\alpha}_n$ are the proton and neutron electric polarizabilities. This differential cross-section depends on the angle of emission, and so, by taking measurements at different angles, proton and neutron polarizabilities can be extracted. Only electric polarizabilities are taken into account in (1.8) for simplicity.

Deuterium was chosen as the target for the scattering experiment due to the fact that no free neutron target exists. Since the deuteron is composed of only a proton and a neutron, it is the easiest to work with. Also, in deuterium, the proton and the neutron are very lightly bound, so the nuclear effects present should be small.

1.4 The Photon Tagger

In order to conduct experiments with photon beams (e.g. the Compton scattering from deuterium) one needs to know the photon energy. Since photons are not charged and have no mass, their energies cannot be measured directly without destroying

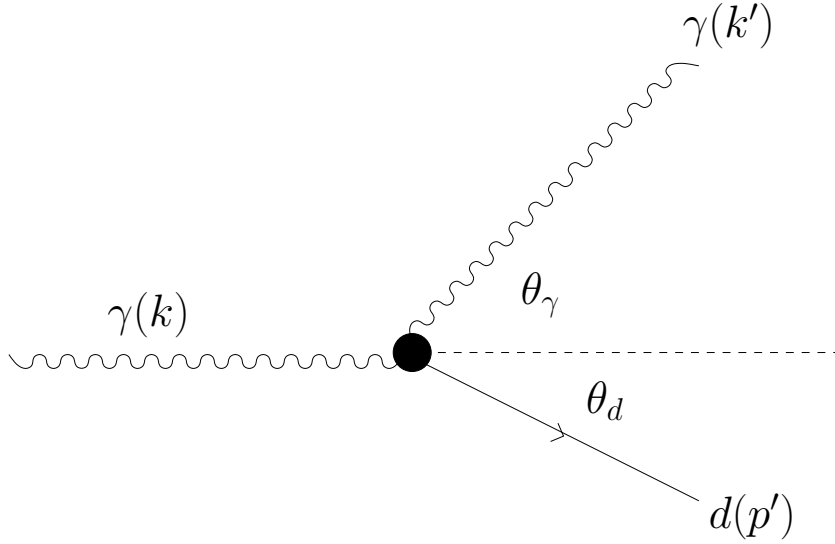


Figure 1.2: Compton scattering from deuterium. $\gamma + d = \gamma + d$.

them. Thus, an indirect method is needed. A common way of producing photons and measuring their energy is called *photon tagging*. It is explained briefly here and then in more detail in Section 2.2. To produce the photon beam needed, an electron beam is directed onto a radiator, which is a thin layer of material, and, through the bremsstrahlung process, the electrons lose energy and emit photons. The bremsstrahlung process produces photons that have a continuous energy distribution, ranging from essentially zero to the energy of the incident electron. Using conservation of energy, the photon energy, E_γ , can be expressed in terms of incident electron energy, E_0 , and post-bremsstrahlung electron energy, E' , as

$$E_\gamma = E_0 - E'. \quad (1.9)$$

The incident electron energy is known, and the residual electron's energy is measured by a large magnetic spectrometer known as the photon tagger, this gives photon energy. This spectrometer is called a photon “tagger” due to the fact that it makes timing coincidences between electrons in the tagger and radiation from the target

(i.e. it “tags” incident photons). This is needed in order to determine which event corresponds to which tagger electron, and in turn, the incident photon energy.

1.5 Photodisintegration of Deuterium

The MAX-lab accelerator lab, where the Compton experiment is to take place, recently installed a new photon tagger and a new accelerator. So, although the purpose of the photon tagger is to provide values for the incident photon energy, the photon energies must be obtained independently from the tagger in order to calibrate it. The photodisintegration of deuterium reaction can provide this.

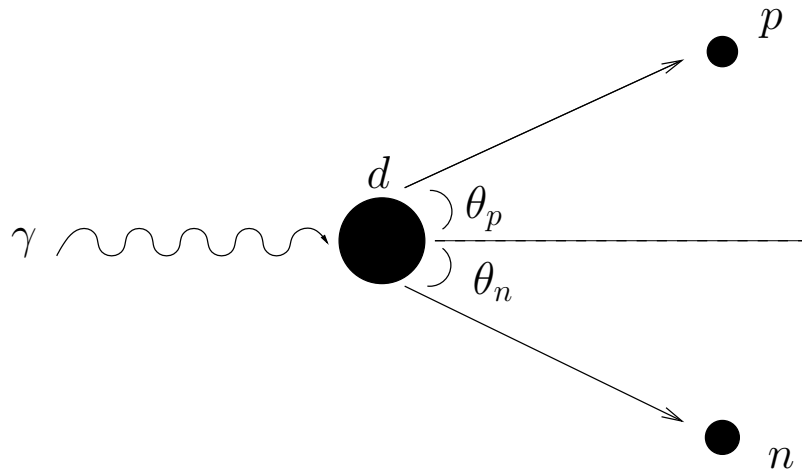


Figure 1.3: The photodisintegration of deuterium, $\gamma + d \rightarrow p + n$.

Deuterium, also known as heavy hydrogen, is an element composed of one proton and one neutron ($Z = 1$, $A = 2$) and has a binding energy of 2.22 MeV. When a photon with sufficient energy is incident upon a deuteron, the bond between the proton and neutron can be broken, emitting them in various directions (see Figure 1.3). Using four-momentum conservation, the energy of the incident photon can be calculated if the emitted neutron kinetic energy and angle of emission (see Appendix A) are

known. The incident photon energy can be expressed as

$$k_0 = \frac{m_p^2 - m_n^2 - m_d^2 + 2m_d(T_n + m_n)}{2 \left(m_d - m_n - T_n + \sqrt{T_n^2 + 2T_n m_n \cos \theta_n} \right)} \quad (1.10)$$

where m_p , m_n and m_d are the masses of the proton, neutron and deuteron, respectively, T_n is the neutron kinetic energy and θ_n is the neutron angle of emission. Using the results from the deuterium photodisintegration measurements, the incident photon energy can be calculated and used to calibrate the photon tagger, which can then be used for other measurements such as the Compton scattering from deuterium to determine the neutron polarizabilities.

Chapter 2

EXPERIMENT

The experiment described in this thesis was conducted at MAX-Lab National Electron Accelerator Laboratory in Lund, Sweden in September 2005. This chapter outlines the apparatus used to carry out the measurement. This includes the accelerator, detectors, data acquisition system and the target.

2.1 MAX-lab Research Facility

MAX-lab [MAX] is a Swedish national laboratory at which three different areas of research are supported: accelerator physics, synchrotron radiation and nuclear physics. The facility consists of three electron storage rings, MAX I, MAX II and MAX III as well as a 500 MeV recirculated electron linear accelerator (LINAC). The beam energies of the storage rings are 0.5 GeV, 1.5 GeV and 0.7 GeV, respectively. These storage rings are used to produce synchrotron radiation, which will not be discussed in this thesis. MAX I can also operate in stretcher mode, which stretches the pulsed beam from the LINAC into a nearly continuous electron beam. A weaker, continuous beam is used as opposed to the pulsed beam so that the data acquisition system does not get overwhelmed with too many events and then sit idle until the next pulse when it is overwhelmed again. This beam is extracted from MAX I and used for the nuclear physics measurements.

2.2 The Tagging System

The stretched beam from MAX I is extracted and transported into the basement to the nuclear physics experimental hall, where it is directed onto a thin radiator. A radiator can be composed of various things, depending on the type of photon beam required. Radiators with a crystal structure, such as diamond, can produce a polarized photon beam, whereas an amorphous radiator, such as aluminum, will produce a nonpolarized beam. A small fraction of electrons will produce photons via the bremsstrahlung process:

$$e^- + N \longrightarrow N + e^- + \gamma, \quad (2.1)$$

where e^- is an electron, N is a nucleus in the radiator and γ is the bremsstrahlung photon. Bremsstrahlung is German for “braking radiation” because this radiation is produced by the acceleration of electrons in the Coulomb fields of nuclei in the radiator. The bremsstrahlung photons will possess energies, E_γ , ranging continuously from zero to the incident electron energy (as seen in Figure 2.1). Energy and momentum are conserved by transfers to the nucleus, but the recoil energy of the nucleus is negligible due to its large mass. Therefore, the energy of the incident beam electron, E_0 , must equal the sum of the post-bremsstrahlung electron (or residual electron) energy, E' , and the energy of the emitted photon. This yields:

$$E_\gamma = E_0 - E'. \quad (2.2)$$

If a timing coincidence can be made between the photon and the residual electron, then the photon is considered “tagged” and its energy can be calculated using (2.2). After passing through the radiator, the electrons enter a large magnetic spectrometer,

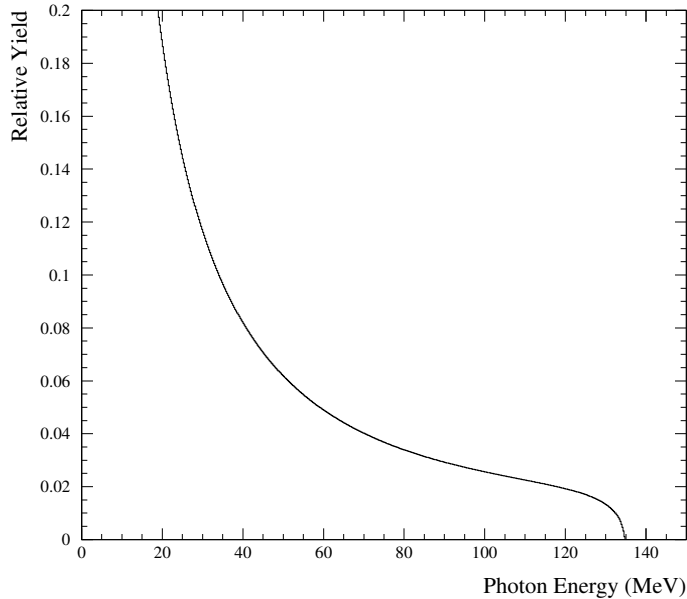


Figure 2.1: Bremsstrahlung energy distribution for a 135-MeV electron beam.

called the tagger magnet. This spectrometer measures the energy of the electrons by directing them onto an array of detectors known as the focal plane. A schematic diagram of the tagger used for this experiment is pictured in Figure 2.2. The Lund focal plane consists of two arrays of 32 plastic scintillator detectors. Electrons that do not produce a photon in the radiator have the same energy as the incident beam and pass by the focal plane into the beam dump. When the electrons enter the magnetic field of the tagger magnet, the trajectory becomes curved due to the Lorentz force, $\vec{F} = q(\vec{v} \times \vec{B})$. Electrons with different energies will have circular trajectories with different radii, shown by,

$$R = \frac{\sqrt{2E'm_e}}{eB} \tag{2.3}$$

with R being the radius of the trajectory, m_e the mass of the electron, e the charge of the electron and B the strength of the magnetic field. Knowing this, all that is

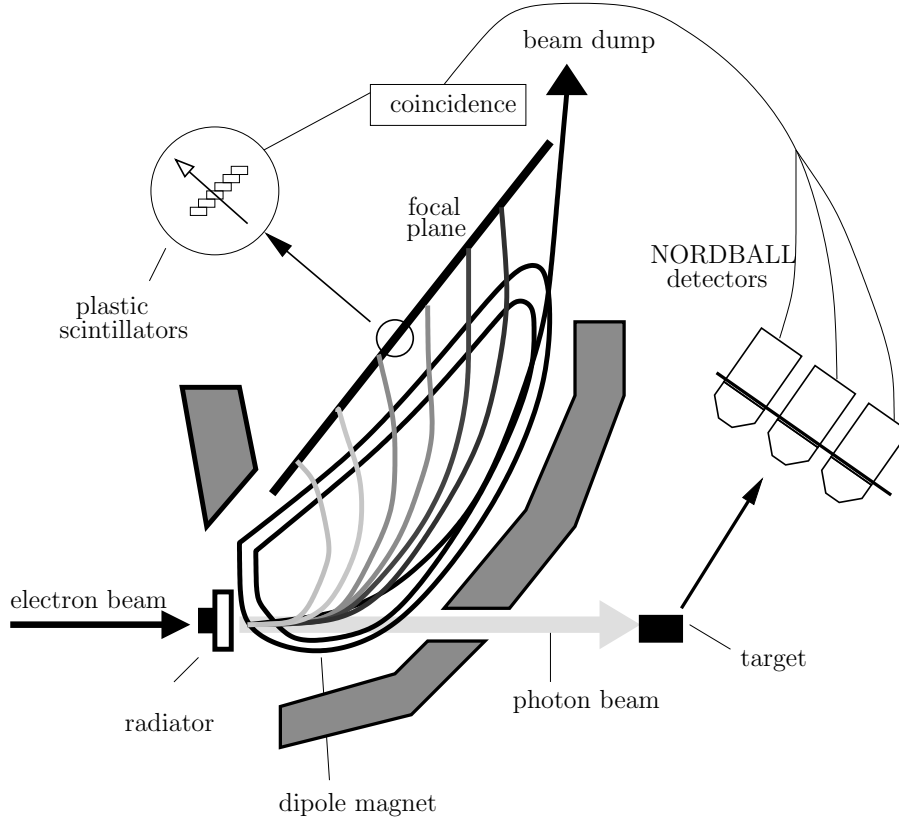


Figure 2.2: Schematic diagram of the Lund Tagger.

needed to calculate the energy of the residual electron is the position of the focal plane detectors. The relationship between position and E' is linear, so the position of the detector hit directly corresponds to the energy of the electron; the energy resolution is defined by the width of the focal plane detectors. When a timing coincidence occurs between an electron in the focal plane and a bremsstrahlung photon, or reaction product thereof, photon energy can be calculated using (2.2).

2.3 NORDBALL Array

Nine NORDBALL detectors were used to detect neutrons in this measurement. NORDBALL detectors are organic liquid scintillation detectors of type BC-501A [Nav05]. They were built at the Chalmers Technical University in Gothenburg, Sweden. The

scintillation medium used is the aromatic hydrocarbon, xylene, with the chemical formula $C_6H_4(CH_3)_2$. Four hexagonal-shaped detectors (3.33 litres) and five pentagonal-shaped detectors (2.57 litres) were used, where the difference between the two shapes is not significant to this experiment. The liquid is contained in a 2-mm thick stainless steel shell and the thickness of the detectors is 160 mm. Each detectors is connected to a photomultiplier tube, type XP-2041, through a 6.35 mm Pyrex glass window. The limiting voltage for these detectors is 3000 V, although they were used with voltages between 1000 V and 2000 V approximately. Each detector operated with a different voltage so that the gains on the detectors were equivalent. They were arranged in three rows, with the center detector being at the same height as the heavy water target (see Figure 2.3).

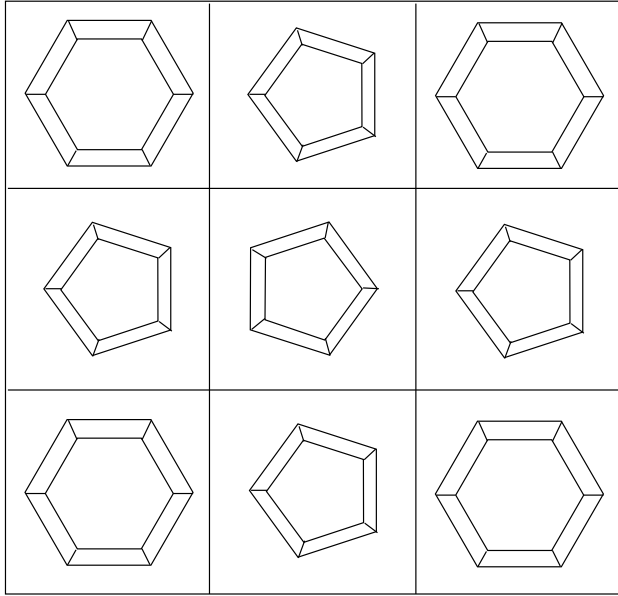


Figure 2.3: Schematic diagram of the NORDBALL detector arrangement.

2.4 Experimental Setup

The deuterium target was placed directly in the path of the photon beam that was produced in the radiator. Heavy water, D_2O , was used as the target and was contained in a small aluminum can. A heavy water target was chosen instead of a deuterium gas (D_2) target due to its larger density which produces a higher count rate for the experiment. Heavy water was chosen over liquid D_2 due to the fact that a liquid D_2 target requires extremely low temperatures and is very difficult to set up and maintain. The NORDBALL detectors were centred at an angle of 122.5° , 3.274 m away from the target (as seen in Figure 2.4). Note that this is the position of the center detector, the positions of the other detectors were slightly different. It was decided the detectors should be placed at a back angle so as to avoid the large amount of γ events present at forward angles. A veto detector, which consisted of a plastic scintillator detector that detected only charged particles, was placed between the target and the neutron detectors. It was configured so that data was only taken for non-charged events (i.e. potential neutrons).

2.5 Measurement

2.5.1 Neutron Time of Flight

In this experiment the kinetic energy of the neutron, T_n , emitted from the deuterium target was calculated by the Time-Of-Flight (TOF) method. The distance from target to detector is known and the time taken for the neutron to travel from the target to the detector, Δt_n , can be calculated and therefore the velocity of the neutrons can be obtained. Since the neutrons measured in this experiment are non-relativistic, their kinetic energy can be calculated from the velocity.

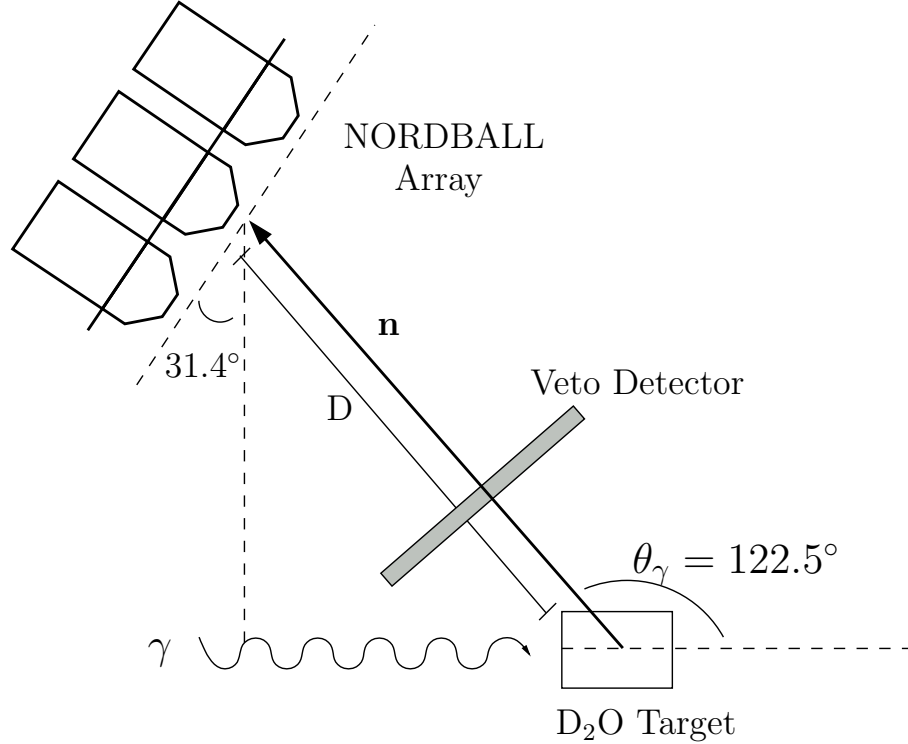


Figure 2.4: Diagram of the placement of the target, veto detector and the NORDBALL detectors.

2.5.2 Neutron Kinetic Energy

Neutron time of flight is not measured directly in this experiment, but is obtained from relative timing with respect to relativistic events. Relativistic particles travel at or near the speed of light, so they have a constant TOF to the target. Therefore they produce a sharp peak at one location on the timing spectrum known as the γ -flash (as shown in Figure 2.5). This peak is constant and provides the relative timing of the neutron flights. To obtain this peak, a 1-mm thick iron plate was used as a target and the veto was set to select charged particles as opposed to filtering them. Note that electrons and positrons were produced in large numbers through pair production and, given their high kinetic energy, were highly relativistic and their velocity was essentially that of the light. These were used to find the location of the γ -flash on the TDC spectra instead of photons because they provided better statistics due to a

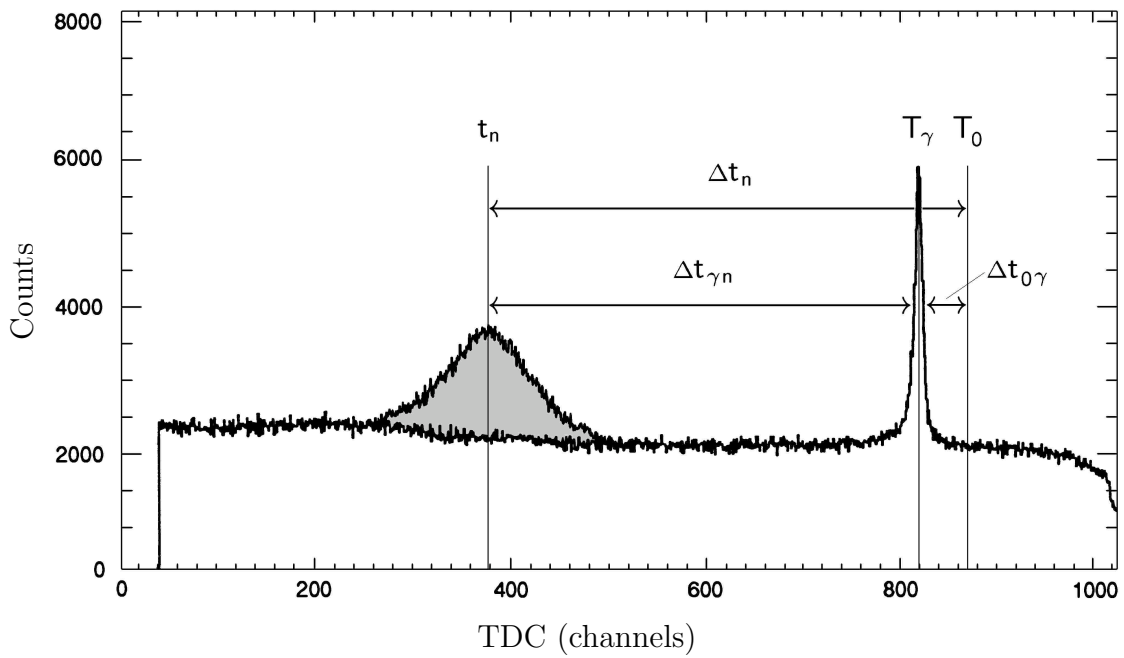


Figure 2.5: The γ -flash produced by relativistic events with the neutron events superimposed. Relative timing of the neutron TOF is shown [Nil06].

higher production rate. The γ -flash occurs at time T_γ with a TOF, $\Delta t_{0\gamma}$, given by

$$\Delta t_{0\gamma} = \frac{D}{c}, \quad (2.4)$$

where D is the target-detector distance and c is the speed of light. The neutron timing can be written

$$\begin{aligned} \Delta t_n &= \Delta t_{0\gamma} + (\Delta t_n - \Delta t_{0\gamma}) \\ &= \Delta t_{0\gamma} + \Delta t_{\gamma n} \end{aligned} \quad (2.5)$$

where

$$\Delta t_{\gamma n} = \Delta t_{\gamma n}(\text{channels})f_{TDC}. \quad (2.6)$$

$\Delta t_{\gamma n}(\text{channels})$ is the number of channels separating the γ -flash and the neutron events on the TDC spectrum and f_{TDC} is the TDC gain in ns/channel. To calculate the kinetic energy of neutron we need the neutron velocity, which is

$$v_n = \frac{D}{\Delta t_n}. \quad (2.7)$$

and the relativistic β of the neutron given by

$$\begin{aligned} \beta &= \frac{v_n}{c} \\ &= \frac{D/\Delta t_n}{c} \\ &= \frac{D/c}{\Delta t_n} \\ &= \frac{\Delta t_{0\gamma}}{\Delta t_n}. \end{aligned} \quad (2.8)$$

This gives a Lorentz factor of

$$\gamma = \frac{1}{\sqrt{1 - \beta^2}} = \frac{1}{\sqrt{1 - \left(\frac{\Delta t_{0\gamma}}{\Delta t_n}\right)^2}} \quad (2.9)$$

which gives a kinetic energy of

$$T_n = (\gamma - 1)m_n c^2 = \left(\frac{1}{\sqrt{1 - \left(\frac{\Delta t_{0\gamma}}{\Delta t_n}\right)^2}} - 1 \right) m_n c^2 \quad (2.10)$$

Thus, knowing the location of the γ -flash and the neutron events on the TDC spectrum will give us neutron kinetic energy.

2.5.3 Pulse-Shape Discrimination

To determine whether an event was a neutron or a photon, a technique called pulse shape discrimination (PSD) was used. PSD is a commonly used technique in nuclear physics that can discriminate between different particles based on the type of light pulse produced in the scintillator detector. Organic scintillators usually emit a light pulse with a fast-decay component and a slow-decay component. These components have different magnitudes depending on the type of incident radiation. Refer to Appendix B for more information on scintillation detectors. A gamma event generally only has a fast-decay component whereas a neutron produces both a fast and slow decay component. To make use of this fact the signals from the neutron cells were split and passed to two different ADCs which integrated the signal. The first was the long-gate (LG) ADC which integrated the first ~ 100 ns of the signal, which is essentially the entire signal. The second signal was sent to a short-gate (SG) ADC which integrated only the first ~ 30 ns of the pulse, which is approximately the amount

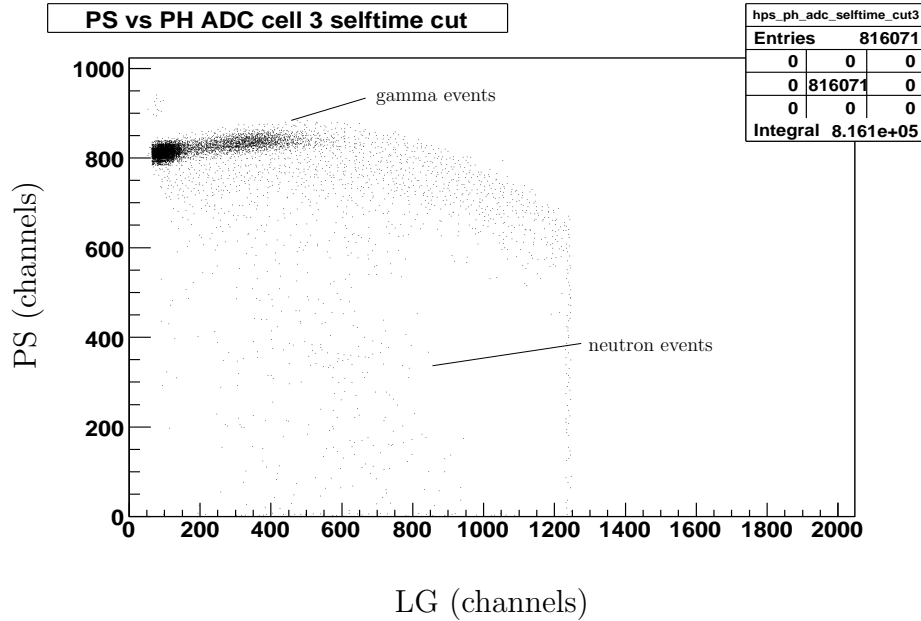


Figure 2.6: Scatter plot of long gate integration versus pulse shape value.

of time needed for the fast-decay component to decay. Seeing as how a γ -event only produces a fast-decay component, the integration provided by both SG and LG ADCs would be the same. For a neutron event though, the SG integration would only include a fraction of the total signal. By comparing these integrations, photon and neutron events could be separated. It should be noted that the LG and SG outputs were not compared directly, but a pulse shape (PS) value was defined as

$$PS = LG - ROT(SG), \quad (2.11)$$

where “ROT” is a scale factor set by a variable attenuator, which was adjusted to maximize neutron/gamma separation. Via a software cut on a scatterplot (Figure 2.6) of PS versus LG, photon events can be eliminated.

2.6 Electronics

The electronics used in this experiment (Figure 2.7) include NIM (Nuclear Instrument Module) electronics, CAMAC (Computer-Automated Measurement and Control) digitizing modules, a VME (Versa Module Eurocard bus) front-end processor, and a data acquisition system running under Linux.

When an event occurs in a detector in the neutron array, the analog signal from the detector is split three ways by a passive splitter. The first signal is sent to the long gate ADC, which integrates the first 100 ns of the analog signal giving the total pulse amplitude. The second is sent to a PSD module which determines whether the signal was a gamma event or a potential neutron event (it should be noted that pulse shape discrimination is used during the offline analysis as well to eliminate γ -events more stringently with software). The analog signal from the PSD is sent to the pulse shape (PS) ADC. The third is sent to a CFD (Constant Fraction Discriminator) which sends a digital signal if the event is above a certain threshold, which eliminates noise from the data (the CFD is triggered by a signal from the PSD module). The signal that leaves the CFD is the OR of all signals from the neutron array. What occurs next depends on the type of particle being observed.

Case: Neutron Event

If the event is a neutron, the output from the CFD is sent to a coincidence with a second signal indicating good beam, which will be explained later. If this coincidence takes place, a signal is sent to the start gate of a latch and the output from this gates the ADCs (veto, long gate, short gate, focal plane), starts the TDCs, as well as being the start signal for a delay unit ($\approx 120 \mu\text{s}$.) The stop signal for the focal plane TDC comes from the focal plane detectors shortly after. The delay gives the modules enough time to perform their various functions and then it sends a signal that generates an interrupt, causing the computer to read in all data. A signal from

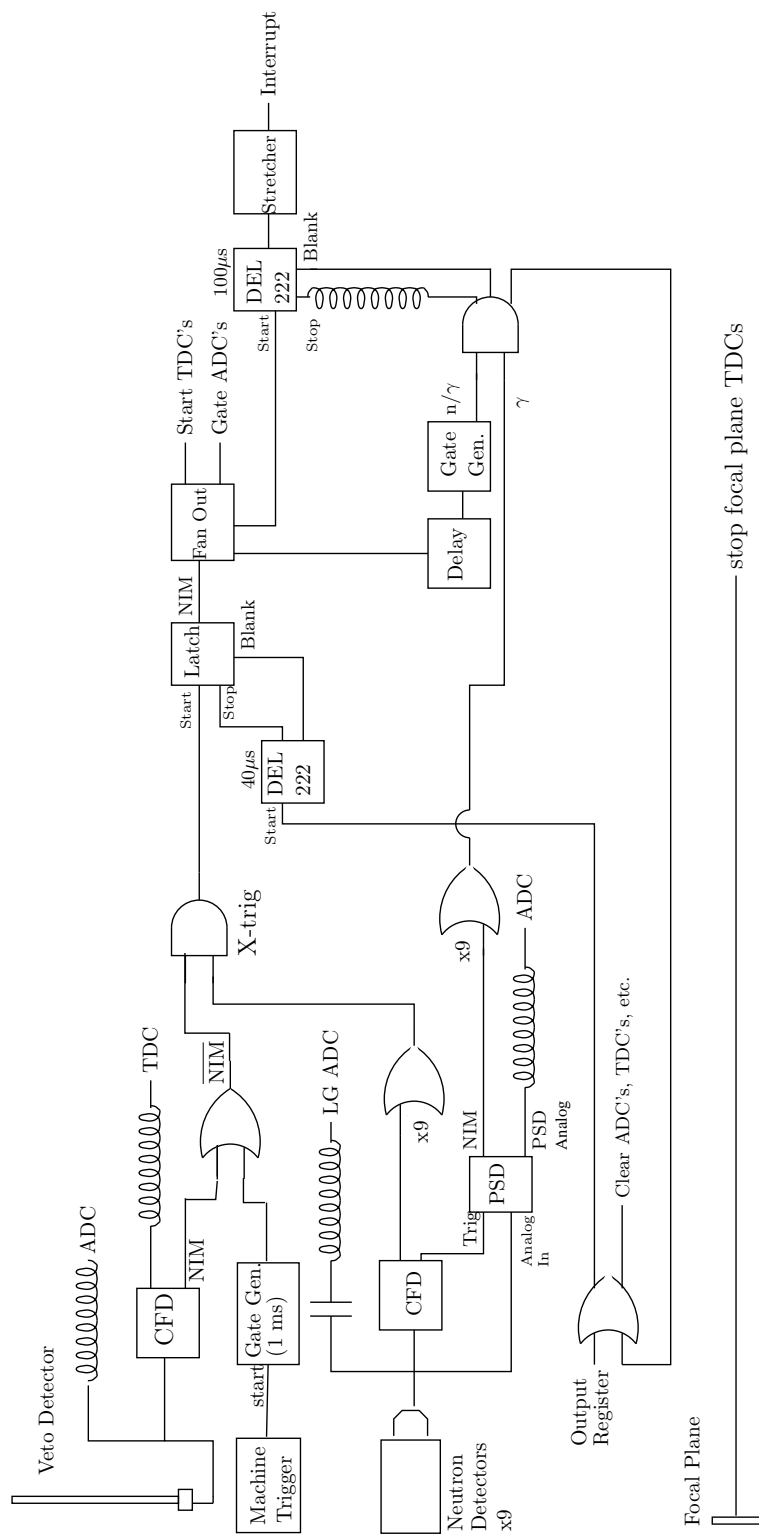


Figure 2.7: Circuit diagram of the data acquisition electronics.

the output register clears the TDCs and ADCs and sends a stop signal to the latch, essentially resetting the whole system so it is ready for the next event.

Case: Gamma Event

In the case where the event occurring in the neutron detector is a photon, the PSD unit will recognize the analog signal from the detector is from a photon. As well as outputting the analog signal to the short gate ADC, a NIM signal will be sent from the PSD unit to a coincidence indicating the γ -event. The other signal in this coincidence is from the latch, indicating a potential event of interest. If this coincidence occurs, the signal will clear all TDCs and ADCs as well as sending stop and blank signals to the 120 μ s delay unit. This ensures that no interrupt is generated and therefore no data is read into the computer.

Case: Charged Particle

If the event is a charged particle (e.g. electron), the particle will trigger the veto detector placed in front of the NORDBALL detectors, as well as triggering the NORDBALL detectors. The analog signal from the veto is split with one going to the veto ADC and the other going to a CFD. The NIM signal from the CFD is inverted and sent to the coincidence with the signal from the same particle coming from the neutron detectors. Since the signal is inverted, the coincidence does not occur, causing the system to wait until another potential event occurs.

It also should be noted that the first millisecond of every twenty milliseconds of beam is ignored. Although the beam from MAX I is stretched, the beam is injected into the storage ring in pulses occurring every twenty milliseconds. Some of the beam does not get stretched and enters the nuclear physics hall in pulses. This burst of electrons would overwhelm the electronics and provide poorer statistics, so a machine trigger is used that sends a signal for the first millisecond of every twenty, identifying the bad beam. This signal is inverted and sent to the same coincidence as the veto.

This ensures that no events are registered during the period.

Chapter 3

ANALYSIS

This chapter will provide the methods by which the incident photon energies were extracted from the results of the photodisintegration of deuterium experiment. This includes PSD event elimination and time of flight calculation. The analysis was conducted using the ROOT software, an object-oriented data analysis framework [ROO]. In Lund there are two different taggers, the main tagger and the end tagger, and there are two different focal planes, the Lund focal plane and a focal plane from the Saskatchewan Accelerator Laboratory (SAL). That data that was analyzed was taken with the main tagger and the SAL focal plane.

3.1 Extraction of neutron events

To isolate the neutron events in the data, a scatterplot was created with pulse shape (PS) versus pulse height (PH) or long gate (LG), as discussed in Section 2.5.3. Neutron events and γ -events could be visually distinguished on this scatterplot. Photon events fell at the top of the scatterplot in a ridge whereas neutron events fell below this ridge. By applying a polygon cut to these scatterplots, unwanted photon events could be eliminated. Figure 3.1 shows the raw PS versus PH plot as well as the plot after the polygon cut was applied. The events not removed by this cut were analysed. Under initial inspection it appeared that the neutron timing was well defined and the value appeared to give a kinetic energy that was approximately correct (see Figure 3.2). The timing was then examined for different tagger channels and it was noticed that it remained at a constant value. Each tagger channel corresponds to a different

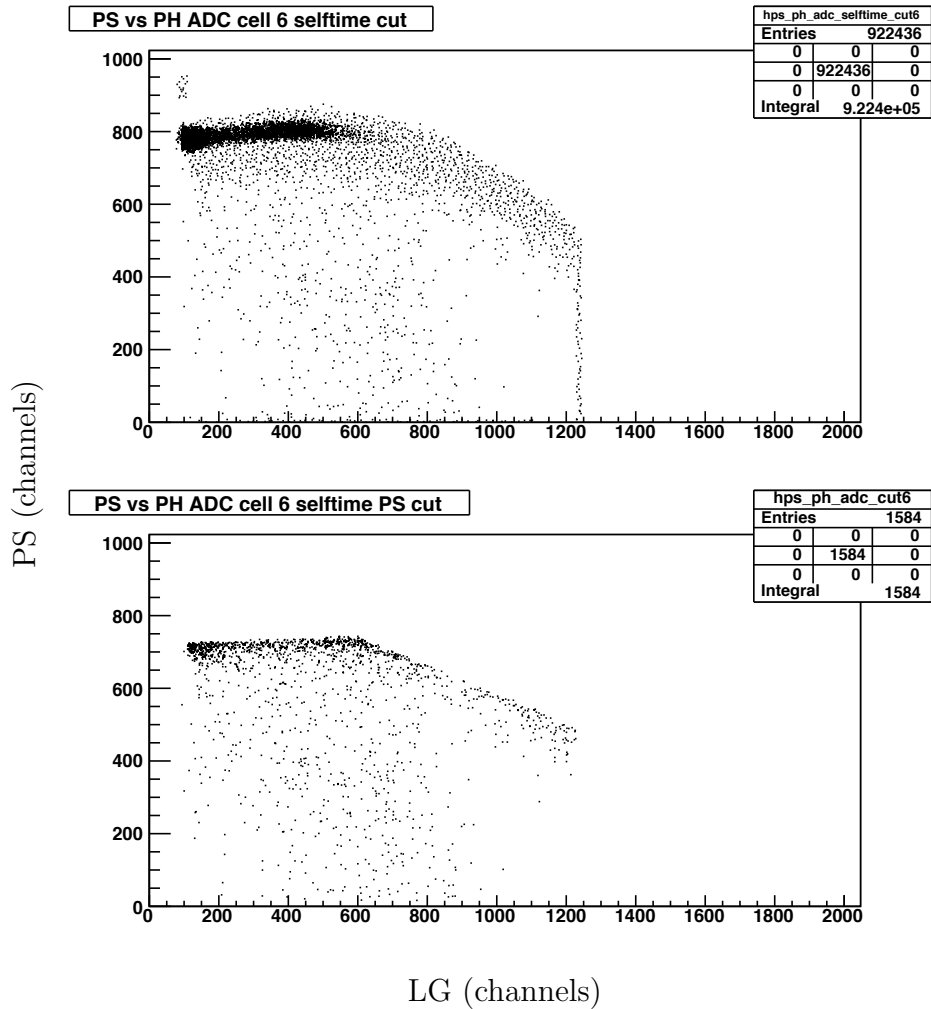


Figure 3.1: Example of the software cut applied to the PS vs. PH scatterplot to eliminate gamma events. The first scatterplot shows the uncut data. The second scatterplot shows the data after the software cut has been applied.

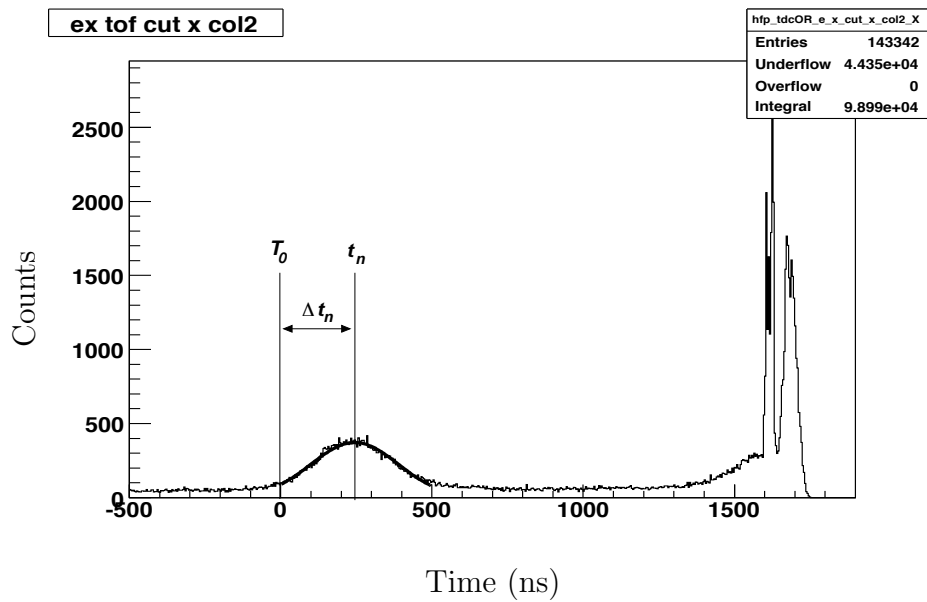


Figure 3.2: Initially the bump seen here was thought to be neutron events and neutron TOF (Δt_n) was measured from the mean of the Gaussian fit shown.

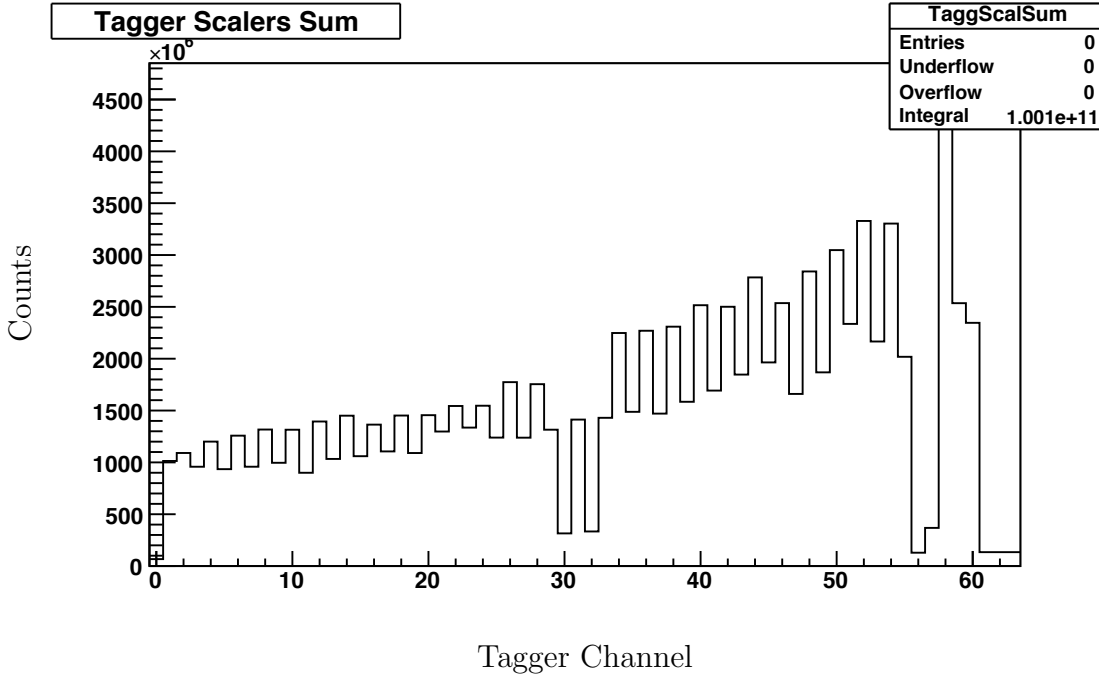


Figure 3.3: Histogram of the scaler values from each channel of the focal plane.

neutron energy, and therefore a different neutron timing should have been observed, but this was not the case. In order to further understand the problem, the heavy water spectrum was compared to a spectrum obtained from normal water. Normal water (i.e. water with ^1H instead of ^2H) does not contain the neutrons that we are trying to eject from the heavy water, and therefore no neutron events should appear. The bump that was initially thought to be neutrons appeared in the normal water spectrum as well though, meaning it was not caused by the neutrons we expected. To overcome this, the spectrum from normal water was scaled and then subtracted from that of heavy water (Figure 3.4) in order to view the difference between the two. To scale the histograms, the ratio of the number of photons incident upon each target was used. This was obtained by integrating the number of electrons in the tagger focal plane (as seen in 3.3) for each target and dividing. The only difference between

the two sets of data should be the presence of emitted neutrons from deuterium in the heavy water set. It should be noted that neutrons are present from the ^{16}O that exists in water, but these neutrons have different energies due to different kinematics, therefore they do not present a problem. A Gaussian fit was applied to the events of interest, the mean value and the sigma value of the fit were provided by ROOT which contains methods for obtaining these values.

3.2 Neutron Time Of Flight

To determine the neutron TOF, focal plane TDC spectra were analyzed. In the TDC spectra of the raw data, the γ -flash occurred at channel 1600 and the time T_0 , the moment at which the reaction actually occurred, was calculated to be at channel 1656. During analysis a corrected TDC spectrum was used. The initial TDC spectrum comes from

$$\Delta t_{TDC} = T_{stop} - T_{start} \quad (3.1)$$

where T_{stop} is provided by the focal plane electrons and the T_{start} signal is from the neutron cells. This gives, from Figure 3.6,

$$\Delta t_{TDC} = \Delta t_e - (\Delta t_t + \Delta t_n) \quad (3.2)$$

$$= T_0 - \Delta t_n, \quad (3.3)$$

where Δt_t is the radiator-target timing, Δt_e is the residual electron flight time, and Δt_n is the neutron TOF. To make the corrected TDC spectrum that was used for analysis the time T_0 was moved to channel zero. This enabled the Δt_n measurement to be made from channel zero to the neutron peak, which occurred at time t_n (see Figure 3.2). This was accomplished by subtracting the initial TDC time from T_0 ,

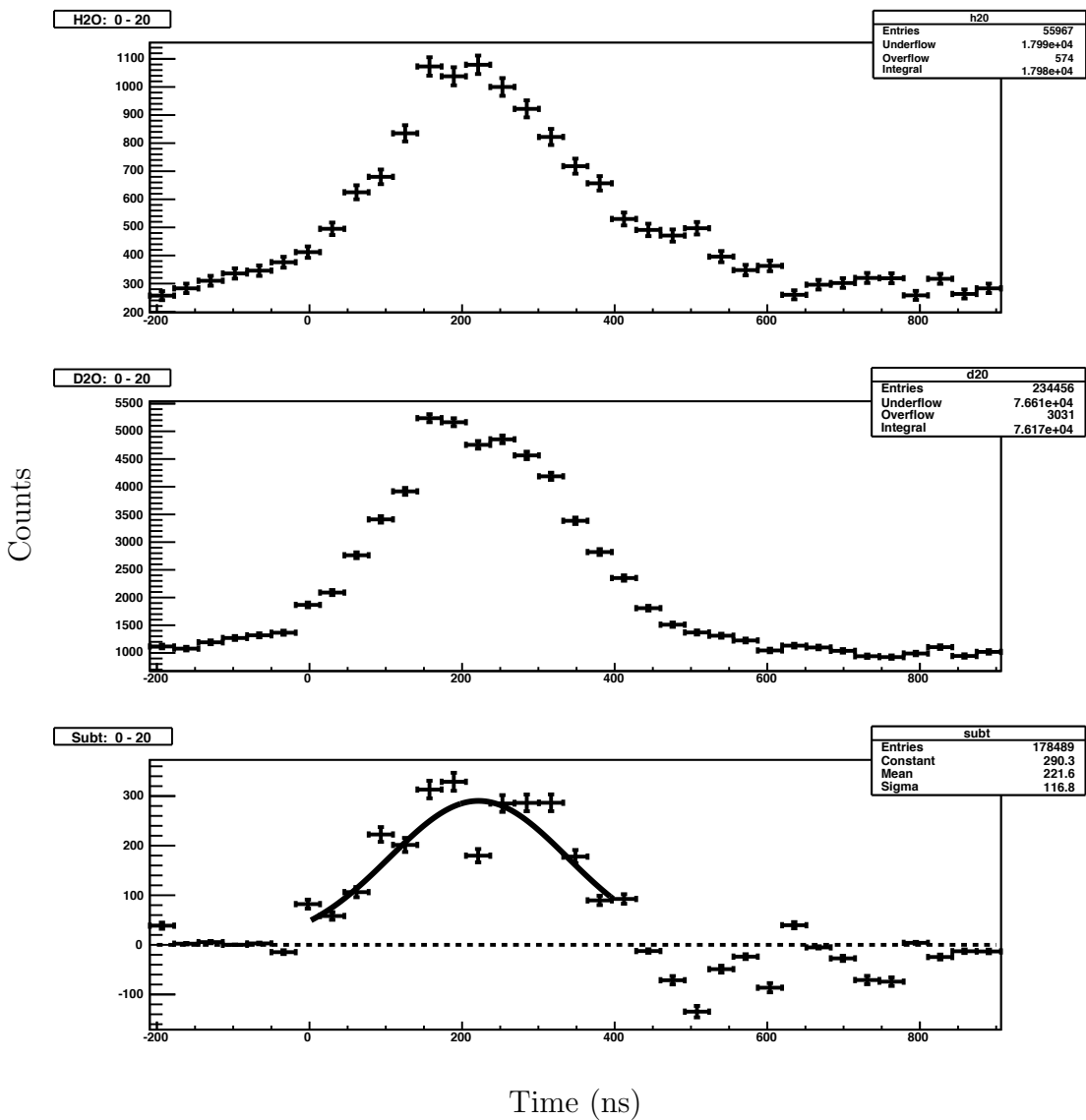


Figure 3.4: The D₂O and H₂O spectrum from focal plane channels 1-21. The bottom histogram is the difference between the two which were scaled by the number of photons needed to produce them.

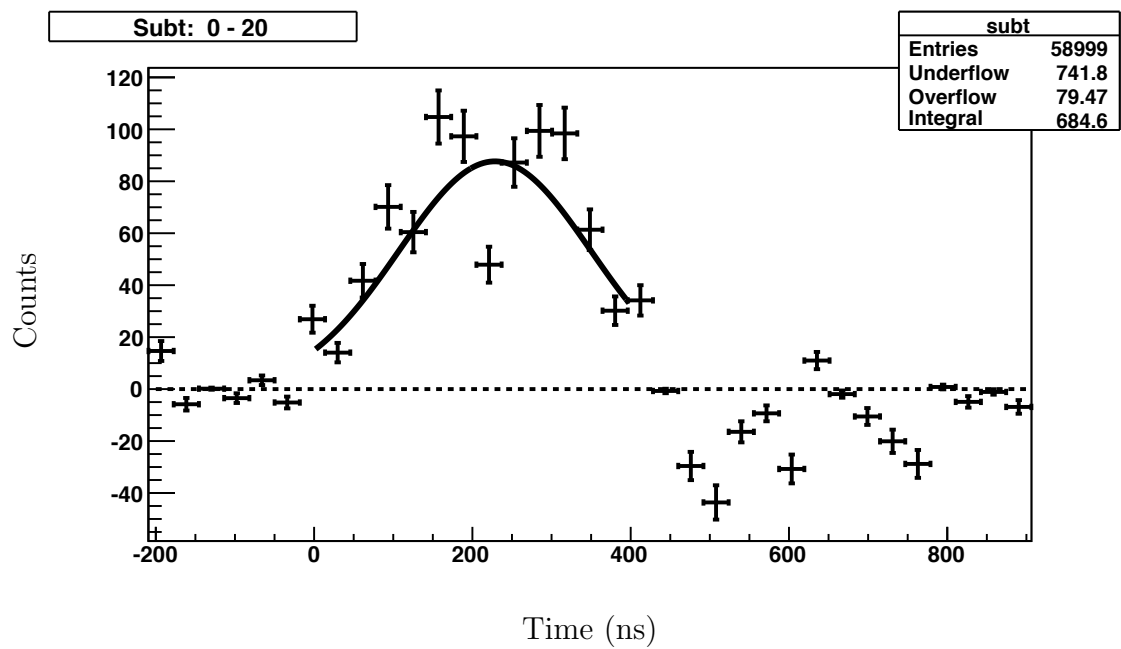


Figure 3.5: A histogram of the H₂O spectrum subtracted from the D₂O spectrum. A Gaussian fit was applied to channels zero to 400. The mean value and the sigma value for the fit are shown on the histogram with corresponding errors.

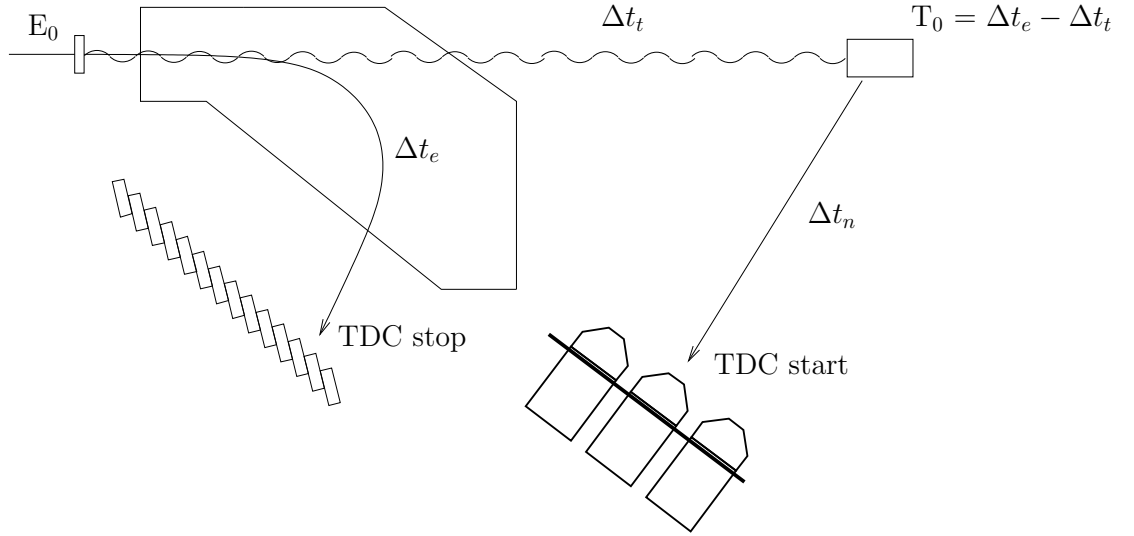


Figure 3.6: Schematic diagram showing the timing of the experiment. Δt_t is the photon time from radiator to target, Δt_n is neutron TOF, T_0 is the time at which the reaction occurs and Δt_e is electron flight from radiator to focal plane.

$$\begin{aligned}
 t_{cor} &= T_0 - \Delta t_{TDC} \\
 &= T_0 - (T_0 - \Delta t_n) \\
 &= \Delta t_n,
 \end{aligned} \tag{3.4}$$

where t_{cor} is the corrected TDC spectrum. Now T_0 is located at channel zero. A Gaussian fit was applied to the neutron bump so as to locate the center of the peak. The focal plane TDCs used were 12-bit (i.e. 4096 channels) and had a full scale of 800 ns. This gives a conversion of 0.195 ns/channel. Using this conversion the neutron TOF could be calculated from the channel number of the t_n peak.

Chapter 4

RESULTS AND CONCLUSION

Due to the low statistics present in the data, the tagger channels were analysed in groups of twenty in hopes of seeing a shift in neutron energies (the last three channels were neglected). After applying a gaussian fit to the three subtracted histograms (channels 0-20, 21-40 and 41-60) the following results were obtained:

Table 4.1: Results from the TDC spectrum analysis.

Tagger Channels	TDC Max	t_n (ns)	T_n (MeV)	E_γ (MeV)
0-20	221.6	43.2	31.5	79.1
21-40	219.4	42.8	32.1	80.8
41-60	224.1	43.7	30.7	77.1
Expected Values				
0	332	64.7	13.6	33
60	243	47.4	25.9	64

Obviously these results do not reflect the change in neutron energy expected from the different tagger channels. The incident photon energies were calculated using (1.10) with an angle $\theta_n = 122.5^\circ$ have a value of about 80 MeV. The expected photon energies range from 33 MeV to 64 MeV and the corresponding neutron values from these are shown in Table 4.1. The expected values were obtained by working backwards from the range of electron energies possible in the focal plane.

4.1 Conclusion

We were unable to find the neutrons in the data from Lund and therefore could not calculate the correct incident photon energies. A large amount of events occurred

approximately where the neutrons should have appeared and, although we tried to remove these events using the normal water spectrum, we were unable to correctly identify the neutrons. It is believed that some beam inconsistency occurred, causing a bombardment of particles that perhaps washed out the neutron events. As was mentioned in Section 2.6, the first millisecond of every twenty is ignored due to beam inconsistencies, though there must be another problem that was not apparent at the time the experiment was being conducted. Also, very little data was available from normal water runs so when the subtraction was performed with normal water, low statistics caused the results to be very poor.

4.2 Future Work

The experiment measuring the Compton scattering from deuterium is expected to run in May 2006 in Lund. To obtain accurate results from this experiment, further work will need to be done in order to calibrate the tagger. If the neutron energies are not obtained from the current data runs, another deuterium photodisintegration experiment will need to be performed.

References

- [Bei03] A. Beiser, *Concepts of Modern Physics*, McGraw-Hill, New York, 2003.
- [Ber93] V. Bernard, N. Kaiser, A. Schmidt, and U.-G. Meissner, *Phys. Rev. Let.* **B319**, 269 (1993).
- [Hal84] F. Halzen and A. D. Martin, *Quarks and Leptons: An Introductory Course in Modern Particle Physics*, John Wiley and Sons, Inc., 1984.
- [Hor99] D. L. Hornidge, *Elastic Photon Scattering from Deuterium*, Ph. D. Thesis, University of Saskatchewan, 1999.
- [Kno89] G. F. Knoll, *Radiation Detection and Measurement*, John Wiley & Sons, Inc., New York, 1989.
- [Lun03] M. Lundin et al., *Phys. Rev. Let.* **90** (2003).
- [MAX] *MAX-lab, Lund University, Sweden*, <http://www.maxlab.lu.se/>, Accessed April, 2006.
- [Nav05] H. Navirian, Measurement of the properties of liquid-scintillator neutron detectors at MAX-lab, M. Sc. Thesis, Lund University, 2005.
- [Nil06] B. Nilsson, J. O. Adler, E. Andersson, J. R. M. Annand, and I. Akkurt, *nucl-ex/0603030* (2006).
- [Olm01] V. M. Olmos de León et al., *Eur. Phys. J.* **A**, 207 (2001).
- [Pes95] M. E. Peskin and D. V. Schroeder, *An Introduction to Quantum Field Theory*, Westview Press, 1995.
- [ROO] *The ROOT System Homepage*, <http://root.cern.ch/>, Accessed April, 2006.

Appendix A

Kinematics

In this appendix the kinematics for the photodisintegration of deuterium will be examined.

The four momentum of a particle has four components and is defined as

$$p = (p_0, i\mathbf{p})$$

where p_0 is the total energy and \mathbf{p} is the linear momentum. Note that natural units are used, i.e. $c = \hbar = 1$. The square of a four-vector, p^2 , is defined by

$$p^2 = p_0^2 - |\mathbf{p}|^2 = m^2 \tag{A.1}$$

where m is the rest mass of the particle. This is invariant under Lorentz transformations. The kinetic energy of a particle can be given as the difference between total energy and the rest mass:

$$T = p_0 - m. \tag{A.2}$$

Also, the total energy of a particle can be expressed as

$$p_0^2 = |\mathbf{p}|^2 + m^2. \tag{A.3}$$

With the above equations the kinematics of the photodisintegration of deuterium can be described. A photon, k , is incident upon a stationary deuteron, d . This results in the disintegration of the deuteron into a proton and a neutron. The neutron is emitted with a momentum, \mathbf{n} , and an angle, θ_n , from the direction of the incident photon. From four-momentum conservation

$$k + d = n + p, \tag{A.4}$$

which can also be written in terms of energy conservation and linear momentum conservation

$$k_0 + d_0 = n_0 + p_0 \tag{A.5}$$

$$\mathbf{k} + \mathbf{d} = \mathbf{n} + \mathbf{p}. \tag{A.6}$$

Rearranging (A.3) and squaring we have

$$\begin{aligned} p^2 &= (k + d - n)^2 \\ p^2 &= (k_0 + m_d + n_0)^2 - (\mathbf{k} + \mathbf{d} - \mathbf{n})^2. \end{aligned} \tag{A.7}$$

In (A.7), m_d is substituted for d_0 because the deuteron has no initial kinetic energy, just rest mass energy. Using (A.2) we get

$$m_p^2 = [k_0 + m_d + (T_n + m_n)]^2 - |\mathbf{n}|^2 + 2|\mathbf{n}|k_0 \cos \theta_n - k_0^2. \quad (\text{A.8})$$

Further, from (A.4), we have

$$|\mathbf{n}| = \sqrt{(m_n + T_n)^2 - m_n^2} = \sqrt{T_n^2 + 2T_n m_n}. \quad (\text{A.9})$$

Finally, combining (A.8) and (A.9) yields:

$$k_0 = \frac{m_p^2 + 2T_n m_n + T_n^2 + 2m_d T_n + 2m_d m_n - T_n^2 - 2T_n m_n - m_n^2 - m_d^2}{2 \left(m_d - m_n - T_n + \sqrt{T_n^2 + 2T_n m_n} \cos \theta \right)}$$

$$k_0 = \frac{m_p^2 - m_n^2 - m_d^2 + 2m_d(T_n + m_n)}{2 \left(m_d - m_n - T_n + \sqrt{T_n^2 + 2T_n m_n} \cos \theta_n \right)}. \quad (\text{A.10})$$

This relationship provides incident photon energy in terms of neutron energy and the angle of emission.

Appendix B

Scintillation Detectors

Scintillation detectors are one of the oldest and most useful tools used in modern nuclear physics. These detectors function based on the properties of certain scintillation materials. In the presence of ionizing radiation these materials emit low energy (usually visible) photons. The scintillation material is coupled to an amplifying device and the photon energy is converted to a electrical signal which can be analysed.

An ideal scintillation material would possess the following properties [Kno89]:

- It should convert the kinetic energy of charged particles into detectable light.
- The conversion from kinetic energy to light should be linearly dependent.
- The material should be transparent to the wavelength of light which it emits so as to have good light collection.
- The decay time of the light pulse should be short so as to generate fast signal pulses.

Although no one material possesses all these properties, different materials have different advantages and should be used depending on the requirements of the experiment.

The excitation of a material resulting in the prompt emission of visible light is known as *fluorescence*. This is the process that is most important in a scintillating material. Other light emission processes can provide useful information about the incident radiation as well and should be recognized. *Delayed fluorescence* yields the same emission spectrum as prompt fluorescence but with a much longer emission time. The ratio between the prompt fluorescence and delayed fluorescence can be used to provide information about the type of incident particle and is known as *pulse-shape discrimination*. *Phosphorescence* yields a longer wavelength of light and usually has a much longer emission time.

B.1 Organic Scintillation

Organic scintillators exist in the form of aromatic hydrocarbon compounds which have vibrational states that can be excited by ionizing radiation. The de-excitation of these states causes the emission of electromagnetic radiation (i.e. a scintillation). Due to the fact that the fluorescence process is a molecular transition, these compounds can be used in various physical states. For example as a vapour, in a solution, or as a solid polycrystalline material.

The de-excitations causing scintillations are the result of free electrons located in π -molecular orbitals. These delocalized electrons do not belong to any one atom

in the molecule and can be excited into any one of a number of molecular excited states. Excited states with spin 0 are the singlet levels (S_0, S_1, S_2, \dots) and excited states with spin 1 are the triplet levels (T_0, T_1, T_2, \dots). Each of the energy levels are further subdivided into smaller vibrational energy levels. The spacing between the electronic energy levels is on the order of a few eV although it decreases with higher energy. The spacing between the vibrational levels is on the order of 0.15 eV (Note: to denote a vibrational energy level a second subscript is used, e.g. S_{00}). The spacing between the vibrational states is still large compared to the average thermal kinetic energy so most molecules at room temperature would be in the ground (S_{00}) state.

When a charged particle or radiation is incident upon the scintillator material, both the electron and vibrational levels are excited. Within picoseconds they decay to the S_{10} without emitting radiation, and this is known as *internal degradation*. From S_{10} there is a high probability of making a transition within a few nanoseconds to one of the excited vibrational states of S_0 . This de-excitation causes a photon to be emitted which is cause of the prompt fluorescence. The intensity of the prompt fluorescence at a given time t can be described by

$$I = I_0 e^{-\frac{t}{\tau}} \quad (\text{B.1})$$

where I is the intensity, I_0 is the initial intensity, t is the time and τ is a time constant. The fact that the S_{10} state decays to one of the excited vibrational states and not the ground state is the reason that scintillators are transparent to the light they emit. The emitted photons lack the energy needed to excite an electron from the S_{00} to the S_{10} so they are transmitted.

Some excited singlets may decay into the first excited triplet state through a transition called intersystem crossing. The lifetime of the T_{10} state can last as long as 10^{-3} s and due to the fact the T_{10} level is lower than the S_{10} level a longer wavelength of light is emitted. This is the phosphorescence component of the scintillation. Triplet states may also interact with each other to produce an excited S state and a ground state molecule which produces the delayed fluorescence.

B.2 Inorganic Scintillation

Inorganic scintillators exist as crystals and the scintillation mechanism used is based on the structure of the crystal lattice of the material. In the crystal structure electrons exist in two discrete bands, the valence band and the conduction band. Electrons existing in the valence band are bound to the lattice sites in the crystal. Those existing in the conduction band have more energy and can travel freely through the crystal. Between these two bands is what is known as the forbidden band, and electrons can never be found there in a pure crystal. Electrons can be excited from the valence band to the conduction band, but the de-excitation back to the valence band with the emission of a photon is inefficient and usually produces photons with a frequency higher than the visible range. To overcome this, small amounts of an

impurity are added to the crystal, called activators. These activators permit energy levels to be created in the forbidden band. Due to the fact that the energy of these levels are less than that of the full forbidden gap, a de-excitation from one will produce a visible photon.

When a charged particle passes through the scintillator it creates many electron-hole pairs. These pairs are created when an electron is excited from the valence band to the conduction band leaving a hole in the valence band. The hole will move to the nearest impurity atom and ionize it because its ionization energy is lower than that of the crystal lattice sites. The excited electron is free to move throughout the crystal and when it reaches an ionized activator, it creates a neutral configuration. If the excited electron has an allowed transition to the ground state it can de-excite and emit a photon. This usually happens almost immediately, on the order of 10^{-7} s. This is the prompt fluorescence portion of the emitted light. It is possible that the electron does not have an allowed transition to the ground state. If this is the case then the configuration will need further excitation to a higher energy state which allows the transition. Usually this is caused by thermal excitations and the light emitted results in the *phosphorescence* portion of the scintillation light.

B.3 Photomultiplier Tubes

Without photomultiplier tubes or other similar devices, used to convert minute light inputs to electrical signals, the use of scintillation materials as detectors would be almost impossible and not nearly as popular. Photomultiplier tubes have two major components with the first being the photocathode, which is a very thin layer of photoemissive material that absorbs the incident photons and converts them to low energy photoelectrons. The photoelectrons then escape the surface of the photocathode. The second major component of a photomultiplier is an electron multiplier structure. They usually consist of a series of electrodes, called dynodes, which have a positive potential greater than that of the cathode. When an electron hits a dynode, more electrons are emitted and travel to the next dynode. This chain of dynodes amplifies the electrons to a useable signal and they are collected at an anode which results in an electric pulse. This pulse can then be analyzed.

B.4 Pulse-Shape Discrimination

The light emission of most scintillators is predominately from the prompt fluorescence and can be described by a simple exponential function given in (B.1). Some scintillators have a large slow component of scintillation light though, and different kinds of incident radiation will yield different amounts of prompt and delayed fluorescence. This slightly more complex pulse can be described by the superposition of two different exponential functions,

$$I = I_A \left(e^{-\frac{t}{\tau_A}} \right) + I_B \left(e^{-\frac{t}{\tau_B}} \right), \quad (\text{B.2})$$

where τ_A and τ_B are constants describing the rate of decay and I_A and I_B are the relative magnitudes. Prompt fluorescence usually decays within 30 ns whereas the delayed fluorescence may have a decay time of 100 ns or more. This difference in magnitude between the prompt and delayed components can be used to determine what kind of radiation was incident upon the scintillator. The most common method is to integrate the signal over two different time intervals (e.g. the first 30 ns and the first 150 ns). A comparison between the long and short integration will yield information about the incident radiation.

RELEASE FORM

To be bound into all copies of theses submitted to
Mount Allison University

AUTHORITY FOR LIBRARY TO REPRODUCE

(To be signed by author)

I hereby authorize the making of copies of this thesis for study purposes.

(Strike out the two statements which are not appropriate.)

A. Without restriction.

B. With the restriction that until _____
_____ Department is required.
(maximum period: five years)

C. With the restriction that until _____
(maximum period: five years)
the written approval of the author is required.

Signed _____
Date _____